Sensors & Actuators: B. Chemical 320 (2020) 128329

Contents lists available at ScienceDirect

Sensors and Actuators B: Chemical

journal homepage: www.elsevier.com/locate/snb

Mixed potential type ppb-level acetaldehyde gas sensor based on stabilized zirconia electrolyte and a $NiTiO_3$ sensing electrode

Jing Wang[a], Li Jiang[a], Lianjing Zhao[a], Fangmeng Liu[a,*], Rui You[b], Siyuan Lv[a], Junming He[a], Zijie Yang[a], Ao Liu[a], Chenguang Wang[a], Xu Yan[a], Peng Sun[a], Geyu Lu[a,*]

[a] State Key Laboratory of Integrated Optoelectronics, Key Laboratory of Advanced Gas Sensors, College of Electronic Science and Engineering, Jilin University, 2699 Qianjin Street, Changchun, 130012 Jilin Province, China
[b] Institute of Microelectronics, Peking University, Beijing 100871, China

ARTICLE INFO

Keywords:
Gas sensor
Acetaldehyde
$NiTiO_3$
Stabilized zirconia

ABSTRACT

An attempt has been performed to develop a selective and sensitive acetaldehyde gas sensor based on yttria-stabilized zirconia (YSZ) solid electrolyte in conjunction with $NiTiO_3$ sensing electrodes (SEs) calcined at different temperatures (800, 1000 and 1200 °C). Among all the evaluated sensing devices, the sensor attached with $NiTiO_3$-SE calcined at 1000 °C was found to have a maximum sensing response value of −43 mV to 50 ppm acetaldehyde and a lower detection limit of 200 ppb at an optimal working temperature of 575 °C. The response and recovery times of the sensing device to 50 ppm acetaldehyde were 10 and 26 s, respectively. The present sensor also exhibited a segmentally linear relationship between the ΔV values and the logarithm of acetaldehyde concentration in the range of 0.2–1 ppm and 1–200 ppm at 575 °C and the sensitivities were −3 mV/decade and −26.5 mV/decade. Furthermore, the developed sensor had a good selectivity, reproducibility, moisture insensitivity, as well as a high temperature stability for 20 days. On basis of the polarization-curve evaluation of the present sensor, the good agreement between the observed values and the estimated values revealed that the sensing mechanism based on mixed-potential model has been confirmed.

1. Introduction

Due to the unceasingly emerging pollution issue for industrial, house miniature environment and atmospheric environment, people pay more and more attention to monitoring different volatile organic compounds (VOCs), which is well known as the common hazardous pollution gases. Acetaldehyde, as one of the most important aldehydes among VOCs with a pungent odour and colorless, is emitted from different combustions and emission processes both indoors (building materials, wood varnish and so on) [1] and outdoors (the exhaust from automobiles and other vehicles) [2]. In another aspect, acetaldehyde classified as group I carcinogen by International Agency for Research on Cancer (IARC) not only plays an important role in environment pollution, but more importantly, it also threatens the human health. It has been stated that the maximum exposure permitted concentration of acetaldehyde is 25 ppm for 8 h work-time as defined by Occupational Safety and Health Administration (OSHA) [3]. Prolonged exposure to acetaldehyde can cause serious adverse health effects, such as eye irritation, headache, the damages of DNA, the alteration of the red blood cell structure and other serious health disorders [4,5]. The above facts necessitate that, there is an urgent demand in the fabrication of highly sensitive and selective acetaldehyde gas sensors, which are capable of reliable, convenient and rapid response to acetaldehyde gas.

Till date, a vast number of research works have performed for the detection of acetaldehyde gas using various methods in different applications, such as liquid/gas chromatography [6,7], amperometric electrochemical cells [8], molecular imprinting technique [9], semiconductor metal oxide sensors [10–12]. More importantly, solid electrolyte type gas sensor with low cost, high response, simple structure, good chemical and mechanical stability is an important and attention-attracting monitoring technology owing to the efficient detection capabilities. At present, the mixed potential type gas sensor based on metal oxides sensing electrode and YSZ solid electrolyte, acknowledged as one of the leading reliable devices, has been extensively used for detection of VOCs and other poisonous gases [13–28]. However, as far as we know, few high performances YSZ-based acetaldehyde gas sensor has been reported. Inspired by such result, the development of acetaldehyde sensors and extended gas detection scope of YSZ solid electrolyte type gas sensors are of the utmost importance and extreme significance.

* Corresponding authors.
E-mail addresses: liufangmeng@jlu.edu.cn (F. Liu), lugy@jlu.edu.cn (G. Lu).

https://doi.org/10.1016/j.snb.2020.128329
Received 3 March 2020; Received in revised form 16 May 2020; Accepted 18 May 2020
Available online 21 May 2020

In this work, we first fabricated three acetaldehyde gas sensors with combination of yttria-stabilized zirconia (YSZ) solid electrolyte and $NiTiO_3$ sensing electrodes (SEs) calcined at different temperatures (800, 1000 and 1200 ℃). The sensor attached with $NiTiO_3$-SE calcined at 1000 ℃ was found to have the highest sensitivity to acetaldehyde at 575 ℃ and the detailed sensing characteristics for the developed sensor were investigated. Moreover, the sensing mechanism was verified by polarization-curve measurement.

2. Experimental

2.1. Preparation and characterization of the sensing electrode material

Nickel (II) nitrate hexahydrate ($Ni(NO_3)_2{\cdot}6H_2O$), Tetrabutyl titanate ($Ti(OC_4H_9)_4$), Ethanol (C_2H_5OH), and Citric acid (CA) were taken as the primary materials for synthesizing $NiTiO_3$ by means of a sol-gel method. All reagents used in this experiment are received from commercial sources and are of analysis grade purity. A typical process for synthesis of $NiTiO_3$ was as follows: First, 5 mmol of $Ni(NO_3)_2{\cdot}6H_2O$ was dissolved in 15 mL of C_2H_5OH under magnetically stirring at room temperature. Second, 5 mmol of $Ti(OC_4H_9)_4$ and 10 mmol of Citric acid were slowly added into the above mixed solution, respectively. Subsequently, 5 mL of deionized water was added to the beaker and the homogeneous solution was formed by continuously stirring for 3 h. Finally, the resultant precursor suspension was maintained at room temperature for 24 h without shaking or stirring. After the completion of reaction, the as-obtained solution was dried at 80 ℃ for 24 h in a vacuum desiccator. After natural cooling to room temperature, the pre-synthesized precursor was calcined at 1000 ℃ for 3 h with a heating rate of 2 ℃/min in a muffle furnace and then the target sample was obtained. For comparison, the $NiTiO_3$ composite oxide materials calcined at 800 and 1200 ℃ were also prepared, respectively.

The crystal and phase structure of the as-prepared samples calcined at different temperatures (800, 1000 and 1200 ℃) were performed by means of Rigaku wide-angle X-ray diffraction analysis (XRD, D/max rA, using Cu Kα radiation at wave length = 0.1541 nm) with a scanning range of $20^\circ - 80^\circ$. Thermogravimetric analysis and differential scanning calorimeter analysis (TG-DSC) of the pre- synthesized precursor was measured using a NETZSCH STA 449F3 simultaneous thermogravimetric analyzer in air from 50 to 1300 ℃ with a heating rate of 10 ℃/min. The surface morphology of the $NiTiO_3$-SE calcined at 800 ℃, 1000 and 1200 ℃ was determined based on a field-emission scanning electron microscope (FE-SEM, JEOL JSM-7500F), operating at 10 kV. Raman spectroscopy of $NiTiO_3$ calcined at 1000 ℃ is recorded in the frequency range of 100–1000 cm^{-1} using LabRAM HR Evolution spectrometer with a laser wavelength of 532 nm. The X-ray photoelectron spectroscopy (XPS) of the $NiTiO_3$ calcined at 1000 ℃ was performed using a Thermo ESCALAB250 spectrometer equipped with an Al-Kα ray source.

2.2. Fabrication and measurement of the acetaldehyde gas sensors

A planar acetaldehyde sensing device was fabricated using a commercial YSZ plate (8 mol% Y_2O_3-doped zirconia, provided by Anpeisheng Corp., China) with the physical dimensions of 2 × 2 mm and 0.3 mm in thickness. The schematic view of the planar YSZ-based acetaldehyde sensor is shown in Fig. 1.

(1) A commercial Pt paste (Sino-platinum Metals Co., Ltd) was printed on both ends of the YSZ plate to obtain a narrow stripe-shaped Pt and a point-shaped Pt. Meanwhile, Pt wire (Diameter of 0.02 mm, purchasing from Sino-platinum Metals Co., Ltd.) was attached to Pt point and Pt stripe as the signal collection leads. Subsequently, the substrate was calcined at 1000 ℃ to get the stripe-shaped Pt reference electrode (RE).
(2) The $NiTiO_3$ sensing materials calcined at different temperatures (800, 1000 and 1200 ℃) were thoroughly mixed with the appropriate amount of deionized water to make it wetting in water and to get uniform sensing electrode pastes, respectively. The resulting paste coated the point-shaped Pt by a small brush was heated to dry and then was calcined at 800 ℃ for 2 h to make a good contact of the sensing electrode with YSZ solid electrolyte.
(3) Temperature controller: The Pt heater with the Al_2O_3 substrate was attached to the reverse side of YSZ plate using an inorganic adhesive (mixture of sodium silicate and alumina powder) with the aim of providing the sensor with the required temperature. Finally, above components were welded to the hexagon socket to obtain integral sensor unit.

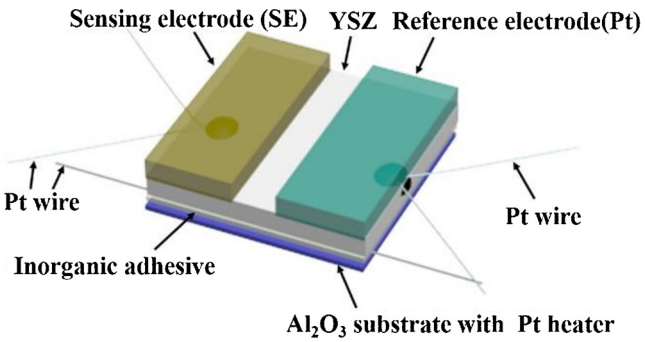

Fig. 1. The schematic view of the planar YSZ-based acetaldehyde sensor.

The gas-sensing properties of the fabricated sensors were evaluated by using a conventional static test method [29]. As previously indicated, The SE and the Pt-RE were connected to the positive and negative terminals of a digital electrometer (Rigol Technologies, Inc., DM 3054, China), respectively. The gas sensing measurement process as follows: Firstly, the developed gas sensor was placed in the airtight chamber with volume of 1 L, which is filled by pure air using an air pump. Then, the sensor was exposed upon another chamber with a certain amount of uniform distribution of sample gas, which was injected into via a special airlock at side of the chamber using a microsyringe. The measurement results were recorded by a computer connected to the electrometer. The sensing signal to sample gas was defined as the difference in the electric potential values (ΔV) between the SE and RE when the fabricated sensors were switched from the air atmospheric to the sample gas and backwards. The desired concentration of sample gas was obtained by the static liquid gas distribution method, which was calculated using the following calculation relation:

$$C = \frac{22.4 \times \rho \times \phi \times V_1}{M \times V_2} \times 1000$$

Where, C is the analyte concentration of the desired target gas (ppm); ρ (g/mL) the density of the injected liquid; ϕ the required gas volume fraction; V_1 (μL) and V_2 (L) the volume of the liquid sample and tested chamber, respectively; and M (g/mol) the molecular weight of the sample liquid. The current-voltage (polarization) curves of the developed sensors were performed by means of the potentiodynamic method (CHI600C, Instrument corporation of Shanghai, China). The electrochemical impedance measurements of different sensing devices were performed using impedance analyzer (Solartron 1260 and Solartron 1287) in 50 ppm acetaldehyde at 575 ℃. The electrochemical impedance measurements of the fabricated sensors were investigated using an impedance analyzer (Solartron 1260 and Solartron 1287) within the frequency range of 100 MHz to 0.1 Hz operating at 575 ℃ in air and each of the tested gases.

3. Results and discussion

The Thermogravimetric analysis and differential scanning

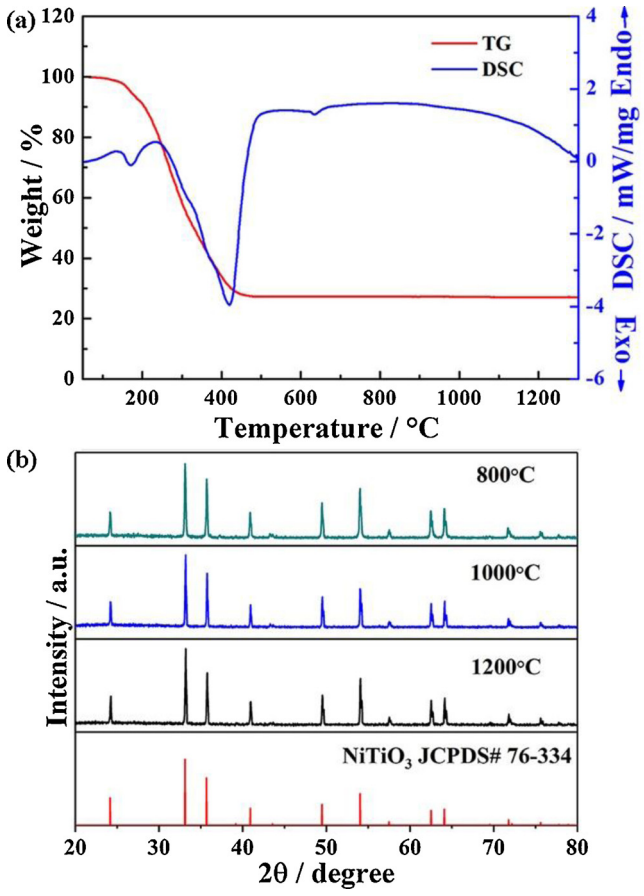

Fig. 2. (a) TG/DSC curves of prepared precursor material; (b) XRD patterns of sensing material sintered at different temperatures.

calorimeter analysis (TG-DSC) of the precursor was performed to investigate thermal stability and to get the suitable calcination temperature of the sensing material. The TG-DSC curves (Fig. 2(a)) of the precursor material indicate two main regions, representing the thermal decomposition behavior. The first region appeared at temperature ranges of 50–140 °C, was probably due to the evaporation of absorption water and the melting of the gel. In the second region, the obvious weight loss at temperature between 140 and 500 °C with slight and remarkable exothermic peaks at about 170 and 420 °C was assigned to the decomposition of the organic components of the precursor and the formation of $NiTiO_3$ phase. Above calcination temperature of 500 °C, almost no mass loss is observed, indicating the formation of stable structure of $NiTiO_3$. Based on obtained measurement result of TG-DSC, X-ray diffraction (XRD) technology was deduced to identify the phase purity and the crystallographic structure of $NiTiO_3$ calcined at 800, 1000 and 1200 °C, and the corresponding measurement results are shown in Fig. 2(b). It is obviously that all the main and sharp diffraction peaks of $NiTiO_3$ materials calcined at different temperatures were coincided with the data from the Joint Committee on Powder Diffraction Standards Card (JCPDS) NO. 76-334 with a rhombohedral structure. In addition, there are no diffraction peaks of other compounds, which shows that a $NiTiO_3$ phase without impurities was obtained at calcination temperature of 800, 1000 and 1200 °C.

Fig. 3(a)–(c) show the surface SEM images of the $NiTiO_3$-SEs calcined at 800, 1000 and 1200 °C. It is clear evidence that the different distribution of the porous surface and nano or micro-dimensional particle of $NiTiO_3$-SEs after calcining at different temperatures were presented. The particle size of the sensing electrode material sintered at 800, 1000 and 1200 °C is about average of 0.3, 0.8 and 1.4 μm, respectively. The particle size of $NiTiO_3$-SEs exhibited gradually enlarge trend with the increase of calcination temperature from 800 to 1200 °C. In order to obtain the corresponding information about the thickness and micro-structure of the cross-section $NiTiO_3$ sensing electrode layer, the cross-section SEM images of the sensing electrodes calcined at different temperature are measured. As shown in Fig. 3(d)–(f), the thickness of the $NiTiO_3$ sensing electrodes calcined at 800, 1000 and 1200 °C was 67, 65 and 64 μm, respectively, which exhibits the similar thickness of sensing electrode layer. Additionally, the porous structure within the sensing electrode layer composed with $NiTiO_3$ calcined different temperatures was also observed. The surface and inside porous channel of $NiTiO_3$ calcined at different temperatures maybe plays an important role for increasing the diffusion efficiency of the tested gas molecules and reducing the gas consumption within the SEs.

The Raman spectrum of the $NiTiO_3$ sensing material calcined at 1000 °C is performed and shown in Fig. 4(a). Ten Raman diffraction peaks located at 190, 227, 244, 290, 343, 393, 462, 482, 611 and 705 cm^{-1} were clearly observed for the $NiTiO_3$ composite oxide sensing material, which consistent with previous reported result with rhombohedral structure of $NiTiO_3$ [30]. The Raman peaks at 190 and 611 cm^{-1} are assigned to Ti – O bond stretching vibrations in the TiO_6 octahedral structure. The Raman peaks at 482 and 705 cm^{-1} may be ascribed to Ni – O – Ti and Ti – O – Ti bond of $NiTiO_3$ [31,32]. The XPS spectra were used for analyzing the chemical composition and the valence state of main elements in the $NiTiO_3$ sensing material obtained by calcination of 1000°C. Fig. 4(b)–(d) exhibited the XPS spectra of survey, Ni 2p and Ti 2p for $NiTiO_3$ sensing material. Clearly, the Ni, Ti and O elements are observed on the surface of $NiTiO_3$ composite oxide, as shown in Fig. 4(b). The XPS high-resolution Ni 2p depicted that the binding energy peaks at 856.1 and 873.7 eV represent the Ni $2p_{3/2}$ and Ni $2p_{1/2}$, respectively. Two satellite peaks observed on the left of main peaks indicate the existence of Ni (II) in a high spin state (Fig. 4(c)) [33]. Fig. 4(d) indicates that the splitting energy of 5.7 eV between Ti $2p_{1/2}$ and Ti $2p_{3/2}$ peaks at 463.9 and 458.2 eV is a typical value for Ti^{4+} [34].

The attempt of further investigate on the different sensing electrode materials which influenced on the sensing performances of the acetaldehyde sensor was undertaken by measuring the response values. Fig. 5(a) shows the response values of the YSZ-based sensors coupled with $NiTiO_3$-SEs calcined at different temperatures (800, 1000 and 1200 °C) upon exposure to 50 ppm acetaldehyde at 575 °C. Comparison between the sensing characteristics of the developed sensors utilizing $NiTiO_3$-SE calcined at 800 °C and $NiTiO_3$-SE calcined at 1200 °C, it can be observed that the sensor coupled with $NiTiO_3$-SE calcined at 1000 °C showed the highest response signal value of −43 mV operating at 575 °C. The reason why the $NiTiO_3$-SE calcined at 1000 °C exhibit the highest response maybe as follows: The appropriate morphology structure of sensing electrode material played an important role for increasing the sensor response. As indicated in Fig. 3, the pore and particle size increased with the increasing calcination temperature. The more porous channels can decrease the consumption of acetaldehyde in the process of diffusion in $NiTiO_3$ electrode layer and facilitate more acetaldehyde gas to reach the TPB (Three Phase Boundary, the interface of $NiTiO_3$ sensing electrode, YSZ solid electrolyte, and Acetaldehyde), which participated directly in electrochemical reactions. In this way, the sensitivity of sensor may be improved with the increasing of sintering temperature. However, the particles of $NiTiO_3$ became too large with the further increase annealing temperature and then the enlarged particle reduced the area of TPB, which results in decreasing active sites, that is, the electrochemical reaction activity of $NiTiO_3$ calcined at 1200°C to acetaldehyde decreased obviously. Thus, the excellent balance of the diffusion of acetaldehyde passed through $NiTiO_3$-SE layer and electrochemical catalytic reaction activity to acetaldehyde is formed when the annealed temperature is 1000 °C. In order to further investigate the reason for the highest sensitivity of the sensor utilizing $NiTiO_3$-SE calcined at 1000 °C, electrochemical impedance spectroscopy (EIS) were tested of the sensor attached with $NiTiO_3$-SE calcined

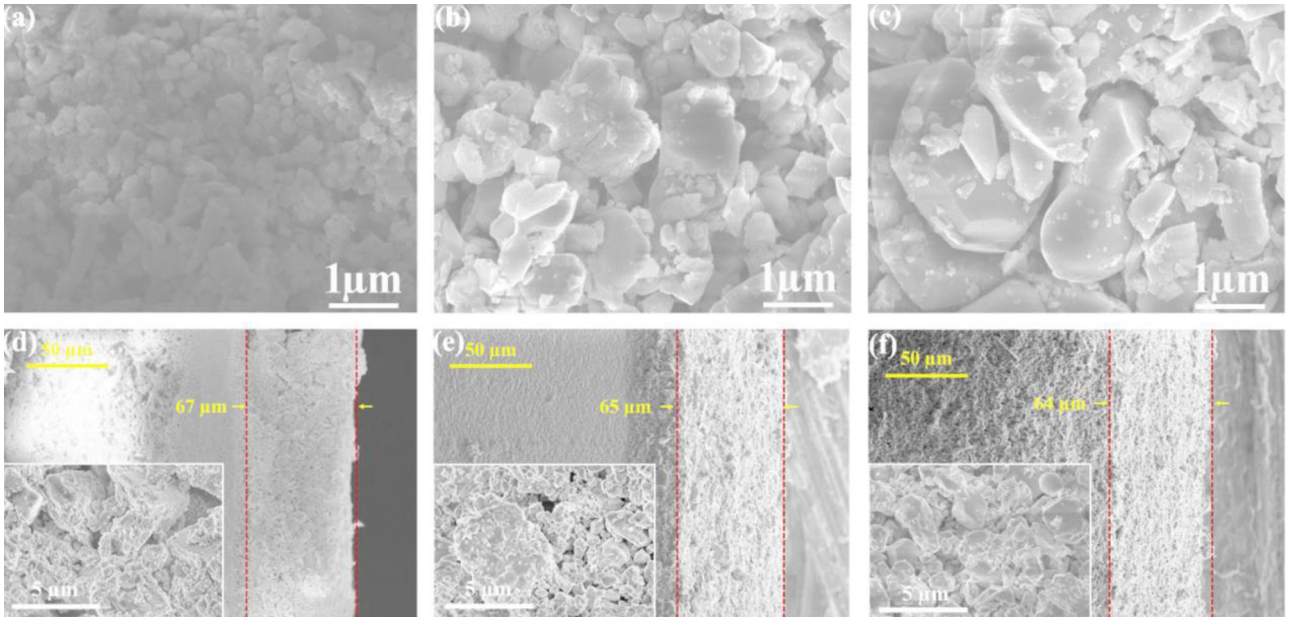

Fig. 3. Surface and cross-section SEM images of $NiTiO_3$-SE calcined at different temperatures (a), (d) 800 °C; (b), (e) 1000 °C; and (c), (f) 1200 °C.

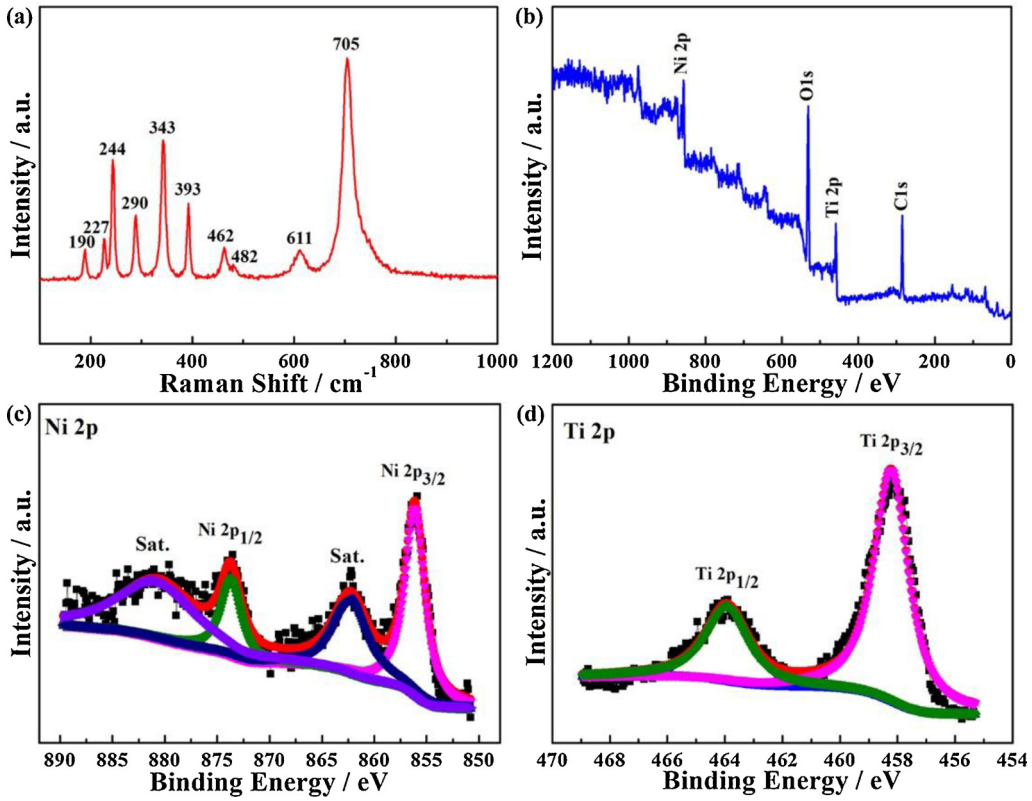

Fig. 4. (a) Raman spectrum of $NiTiO_3$ sensing material obtained at calcination temperature of 1000 °C and XPS spectra of $NiTiO_3$: (b) survey; (c) Ni 2p; (d) Ti 2p.

at different temperatures in air and 50 ppm acetaldehyde operating at 575 °C and shown in Fig. 5(b). Based on reported previously [35–38], the resistance at higher frequencies for the fabricated sensor is mainly contributed to $NiTiO_3$-bulk resistance (including the small YSZ-bulk resistance). And the interfacial resistance is given by the resistance value at the intersection of the large semi-arc with the real axis at lower frequencies (around 0.1 Hz). The equivalent circuit and the corresponding circuit parameters were determined, as shown in the inset of Fig. 5(b). Here, R_0 is the YSZ-bulk resistance; R_{se} and C_{se} mean the resistance and capacitance of composite oxide sensing electrode, respectively; R_{ct} and C_{ct} are the resistance and capacitance of interface between sensing electrode and YSZ solid electrolyte, respectively. Obviously, it seems that the electrode resistance is affected by using different calcination temperatures and the interfacial resistance is changed in air and 50 ppm acetaldehyde. When the sensor attached with $NiTiO_3$-SE calcined at 1000 °C was exposed to air and 50 ppm acetaldehyde, the electrode resistance at the higher frequency and the interfacial resistance at the lower frequency were obviously decreased, comparing

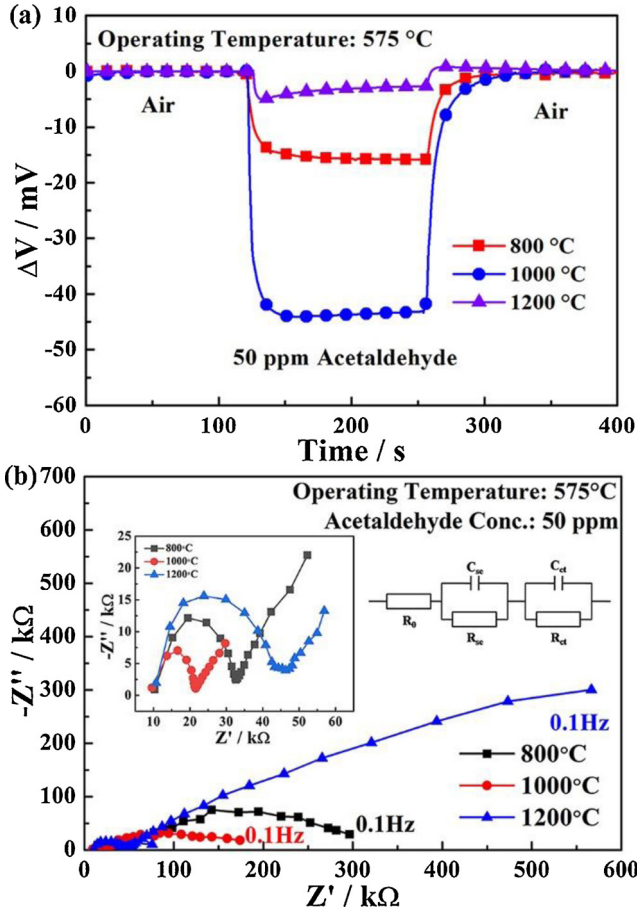

Fig. 5. (a) Response and recovery characteristics of sensors utilizing $NiTiO_3$-SEs calcined at different temperatures to 50 ppm acetaldehyde at 575 °C; (b) Electrochemical impedance curves in 50 ppm acetaldehyde for the sensor attached with $NiTiO_3$-SE calcined at 800, 1000 and 1200 °C operating at 575 °C (inset image depicts the high frequency range).

with sensors using $NiTiO_3$-SE calcined at 800 and 1200 °C. And the electrode resistance of the sensor calcined at the same temperature is rarely affected by the air and tested acetaldehyde. Changes in the interfacial resistance measured of the sensors annealed at different temperatures revealed the electrochemical catalytic activity toward the examined gases [39,40]. Clearly, the interfacial resistances of the sensor attached with $NiTiO_3$-SE calcined at 1200 °C in air and 50 ppm acetaldehyde are much higher than those of sensors using $NiTiO_3$-SE calcined at 800 and 1000 °C, which displayed the lowest sensing response due to the lowest electrochemical catalytic activity to air and acetaldehyde (Fig. S2). Additionally, the sensor attached with $NiTiO_3$-SE calcined at 1000 °C exhibited the lowest interfacial resistance and largest change of interfacial resistance in the air and in the acetaldehyde comparing with other sensing devices. Thus, it can be speculated that the electrochemical catalytic activity of the sensor using $NiTiO_3$-SE calcined at 1000 °C to acetaldehyde was highest, which generated the largest sensing performance toward acetaldehyde. Hence, the sensor utilized $NiTiO_3$-SE calcined at 1000 °C is used as a potential candidate for monitoring acetaldehyde and was further investigated in the following content.

The response and recovery curves toward 100 ppm acetaldehyde were tested in the working temperatures range of 525–625 °C to assess the best operating temperature of the fabricated sensor. As we can see from Fig. 6, the sensor attached with $NiTiO_3$-SE calcined at 1000 °C exhibited a raised tendency to 100 ppm acetaldehyde as the working temperature increasing at the beginning. The sensor was found to be capable of the maximum response value to acetaldehyde at an

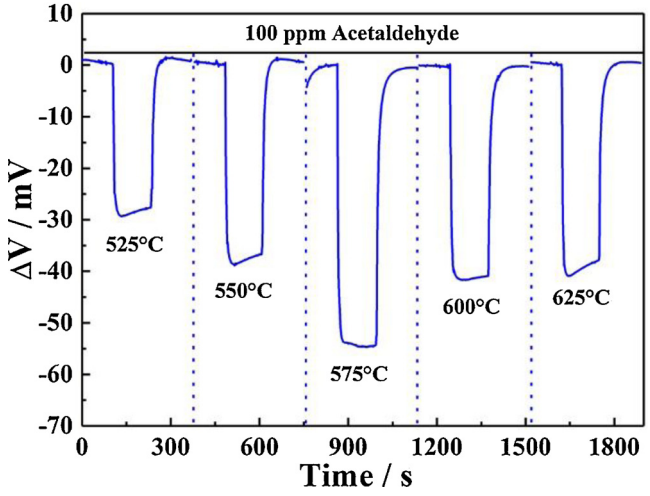

Fig. 6. Effect of the operating temperature on response value of the sensor based on $NiTiO_3$-SE calcined at 1000 °C to 100 ppm acetaldehyde.

operating temperature of 575 °C. After that, the response value declined with the increase working temperature. Therefore, the response value of the fabricated sensor varies with an "increase-maximum-decay" tendency. The improved activation degree can give explanations for the reason of this phenomenon. At the lower working temperature (< 575 °C), the activation energy for electrochemical reaction is deficient, leading to a poor response. With increasing the working temperature, the improved sensing response was achieved, due to the quick acceleration of the electrochemical reaction at TPB. While further increasing the working temperature, the desorption process of acetaldehyde proceeds dominant, and cause the amount of acetaldehyde adsorbed on the SE to decrease, which lead to deterioration of response at higher temperature. Hereafter, the sensing performances of the developed sensor would be examined at 575 °C.

Fig. 7(a) shows the response and recovery curves for the YSZ-based sensor attached with $NiTiO_3$-SE calcined at 1000 °C upon exposure to different concentrations of acetaldehyde ranging from 0.2 to 200 ppm. The test time keep identical during each examined situation in the air or in the acetaldehyde gas. When acetaldehyde gas is exposed on the surface of the sensor, the response value was defined as sensing signal at last minute. It is noted that the sensor to each measured acetaldehyde concentration can respond fast before and after the introduction of acetaldehyde vapor. The response value of the sensor toward 100 ppm acetaldehyde was about −54.5 mV at 575 °C, which is apparently higher than those of Pt/SnO_2 sensing electrode doped with other oxide materials [41]. The detection limit was 200 ppb acetaldehyde with the response value of −1.4 mV. The response and recovery times of the sensing device to 50 ppm acetaldehyde were 10 and 26 s, respectively (Fig. 7(b)). In addition, the dependence of ΔV on the logarithm of corresponding acetaldehyde concentration for the sensor coupled with $NiTiO_3$-SE calcined at 1000 at 575 °C are shown in Fig. 7(c). The observed results revealed that the sensitivity of the present sensor varies sectionally linearly relationship with the logarithm of acetaldehyde concentration within the range of 0.2–1 ppm and 1–200 ppm, and the slopes were −3 mV/decade and −26.5 mV/decade, respectively. The reason for different linearity relationship could be explained as follows: It has already reported that the concentration of acetaldehyde at the TPB and the number of reaction site of the TPB, at which the electrochemical reaction occurred, can affect the sensing signal of the developed sensor. At low concentration of acetaldehyde (0.2–1 ppm), the number of TPB reaction site obtained was high enough to provide the electrochemical reaction. Apparently, enhanced sensing response of the sensor is mainly attributed to the amount of acetaldehyde, which reached on the TPB and involved in the electrochemical reaction. The

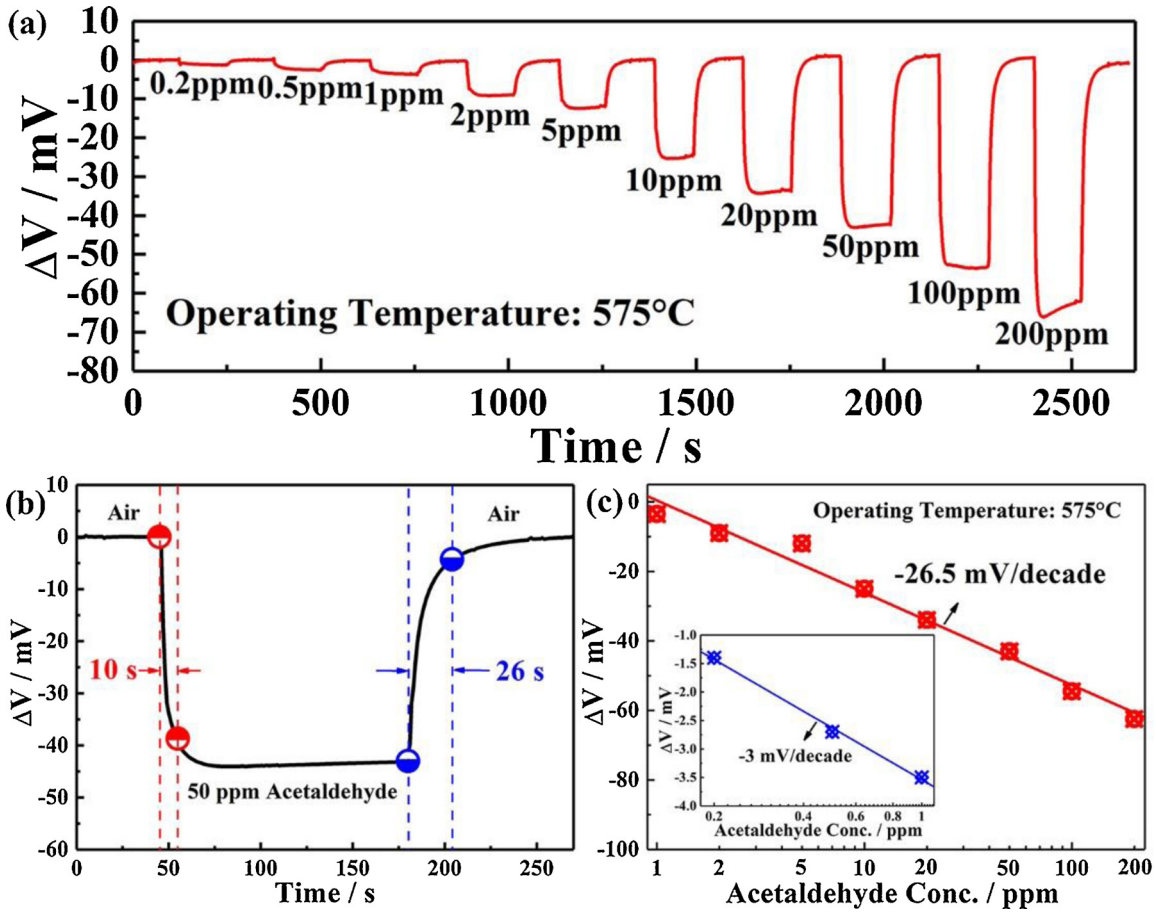

Fig. 7. (a) Response transients of the sensor utilizing $NiTiO_3$-SE calcined at 1000 °C toward 0.2–200 ppm acetaldehyde at 575 °C; (b) Response and recovery curve of the sensor to 50 ppm acetaldehyde; (c) Dependence of ΔV for the present sensor on the logarithm of acetaldehyde concentration at 575 °C.

porosity structure of the $NiTiO_3$-SE can lead to the acetaldehyde gas diffusion through its structure into the TPB and participate in electrochemical reaction. However, some amount of acetaldehyde gas was also consumed in the process of passing through the $NiTiO_3$-SE layer. Upon exposure to measured concentration of acetaldehyde ranging from 0.2 to 1 ppm, the consumption in the process of diffusion played more important role than that at high acetaldehyde concentration (1–200 ppm). Hence, the relatively lower sensitivity was obtained toward low acetaldehyde concentration in compared with that of higher concentration.

To confirm the stability of sensing signal reproducibility during multiple continuous measurement process, the continuous response and recovery performance of the sensor to 100 ppm of acetaldehyde at 575 ℃ was investigated, the result of which is given in Fig. 8(a). It is demonstrated that the present sensor is able to generate almost constant response values during continuous 5 cycles, confirming that the sensor coupled with $NiTiO_3$-SE calcined at 1000 °C processed a good reproducibility toward acetaldehyde gas. For a practical application as acetaldehyde sensor, the cross-sensitivity is a key sensing property index. Besides acetaldehyde, other pollutants, such as C_2H_2, NO, NH_3, NO_2, CO, Benzene, Toluene, Acetic acid, Xylene, Methanal, Ethanol, and Methanol are often coexisted in realistic atmospheric environment. The response values of the developed $NiTiO_3$-SE sensor toward different tested gases of 100 ppm at the same experimental conditions were investigated and the result is given in Fig. 8(b). The sensor generated relatively higher sensing response and selectivity to 100 ppm acetaldehyde than those to other evaluated interference gases at 575 ℃. This confirmed that the developed sensor coupled with $NiTiO_3$-SE calcined at 1000 ℃ displayed good selectivity to acetaldehyde, and was capable of being a practical candidate sensor for monitoring acetaldehyde. To comprehend the selectivity of the sensor, the impedance properties of the sensor attached with $NiTiO_3$-SE calcined at 1000 °C to different gases (Air, 100 ppm Acetaldehyde, 100 ppm Ethanol, 100 ppm Benzene, and 100 ppm CO) were investigated, as shown in Fig. S3. Remarkably, the interfacial resistance of the sensor at the lower frequency range in 100 ppm acetaldehyde was obviously lower than those in 100 ppm ethanol, 100 ppm benzene and 100 ppm CO, which represents the highest electrochemical catalytic activity to acetaldehyde. In this regard, the highest sensing response of the sensor toward acetaldehyde can be achieved. Impedance analysis result is consistent with the measurement data of response values in selectivity and further verify good selectivity for the sensor attached with $NiTiO_3$-SE calcined at 1000 °C to 100 ppm acetaldehyde at 575 °C. The sensor usually works in a realistic working condition where the humidity fluctuating. Aiming at realizing their practical application, the effect of different relative humidity (20%–98% RH) on the acetaldehyde sensing response for the YSZ-based sensor in conjunction with $NiTiO_3$-SE calcined at 1000 ℃ is discussed. The acetaldehyde gases with different relative humidity are obtained at 25 °C by the humidity chamber (Shanghai ESPC Environment Equipment Corporation, China). It is clearly observed from Fig. 8(c) that the response signal value of the developed sensor to 100 ppm acetaldehyde in the range of 20%–98% RH exhibited certain slight fluctuation with the changes of the water vapor concentration.

Furthermore, a potential sensor is usually used for long-time monitoring acetaldehyde. Thus, the stability of the sensor using $NiTiO_3$-SE calcined at 1000 ℃, as a vital characteristic, is studied in 100 ppm acetaldehyde over a period of 20 days at 575 ℃. The response value was evaluated every other day during the long-term tested period. As given

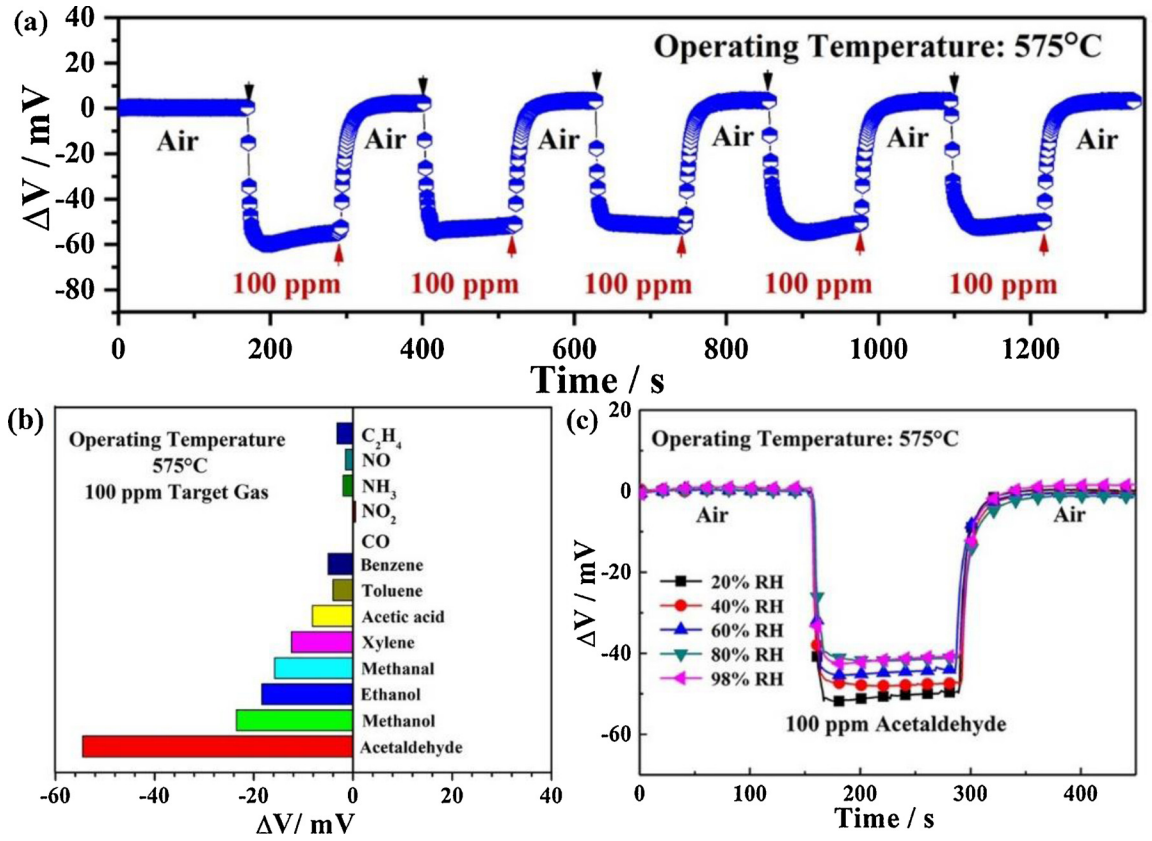

Fig. 8. (a) Response transients of the sensor using $NiTiO_3$-SE calcined at 1000 °C to 100 ppm acetaldehyde during continuous 5 cycles at 575 °C; (b) Selectivity of the sensor to 100 ppm various gases; (c) Response and recovery curves of the sensor to 100 ppm acetaldehyde in the range of 20%–98% RH.

in Fig. 9, there was no serious drift and change in response value of the developed sensor during 20 days of high temperature operation. In order to check the change of the response value (ΔV_s) for the device, the ΔV_s was defined as follows: $\Delta V_s = [(\Delta V_n - \Delta V_0)/\Delta V_0 * 100\%]$, where ΔV_n is the response signal at the following 20 day test period and ΔV_0 is the acetaldehyde response at the starting day. The response value for the sensor towards 100 ppm acetaldehyde was almost unchanged during the high temperature of 20 days measurement and the maximum response variation was 4.6%. In addition, the response and recovery transients for the fabricated sensor to 100 ppm acetaldehyde on the initial, 10th and 20th day showed good consistency. Furthermore, the average value of response with an error bar by measuring multiple times was also consistent with each other during the long-term measurement process of 20 days (Fig. S4). Consequently, the developed sensor based on $NiTiO_3$-SE calcined at 1000 °C was capable of a good stability to acetaldehyde over working period of 20 days at 575 °C.

Furthermore, in order to confirm the developed gas sensor operating at the mixed-potential sensing mechanism, the polarization-curves of the device attached with $NiTiO_3$-SE calcined at 1000 °C was measured in air and different concentration levels of acetaldehyde vapor (50 and 100 ppm) and displayed in Fig. 10. The estimated values (−41.5 and −53.5 mV) are in good coincidence with observed values (−43 and −54.5 mV), which verified the present sensor was governed by the mixed-potential model [42–44]. Based on above results, when the sensor was upon exposure to acetaldehyde gas, the mixed-potential occurred on the TPB according to dynamic balance between the following cathodic reaction of oxygen (1) and the anodic reaction of acetaldehyde (2):

$$\text{Cathodic reaction: } O_2 + 4e^- \rightarrow 2O^{2-} \quad (1)$$

$$\text{Anodic reaction: } 2/5CH_3CHO + 2O^{2-} \rightarrow 4/5CO_2 + 4/5H_2O + 4e^- \quad (2)$$

The sensor was treated quantitatively according to Butler-Volmer equation [17,45], the mixed potential (V_M) is represented by following Equation under the constant O_2 concentration:

$$V_M = V_0 - nA \ln C_{Acetaldehyde} \quad (3)$$

V_M varies negative linearly with an increase of the concentration logarithm of acetaldehyde, which is in accordance with the result in Fig. 7(c). Such theoretical analysis results further demonstrated that the present sensor abided by the mixed potential sensing mechanism.

4. Conclusion

In summary, $NiTiO_3$ sensing electrode synthesizing by facile sol-gel method is used for fabricating an yttria-stabilized zirconia (YSZ)-based mixed potential type acetaldehyde sensor. Among different $NiTiO_3$-SEs calcined at various temperatures (800, 1000 and 1200 °C), the sensor coupled with $NiTiO_3$-SE calcined at 1000 °C is found to show the highest sensing response to 50 ppm acetaldehyde and the detection limit of 200 ppb at 575 °C. The ΔV of the developed sensor varied sectionally linear on a logarithmic scale of acetaldehyde concentration ranging from 0.2 to 1 ppm and 1–200 ppm, with the slopes of −3 mV/decade and -26.5 mV/decade, respectively. Moreover, the sensor exhibited rapid response, good reproducibility, selectivity, long-term stability for 20 days and slight influence of the water vapor to acetaldehyde. Due to the above-mentioned excellent sensing characteristics, the developed sensor attached with $NiTiO_3$-SE calcined at 1000 °C is suggested as one of the promising solid-state device candidates for sensitive detection of acetaldehyde in the atmosphere.

CRediT authorship contribution statement

Jing Wang: Conceptualization, Data curation, Formal analysis,

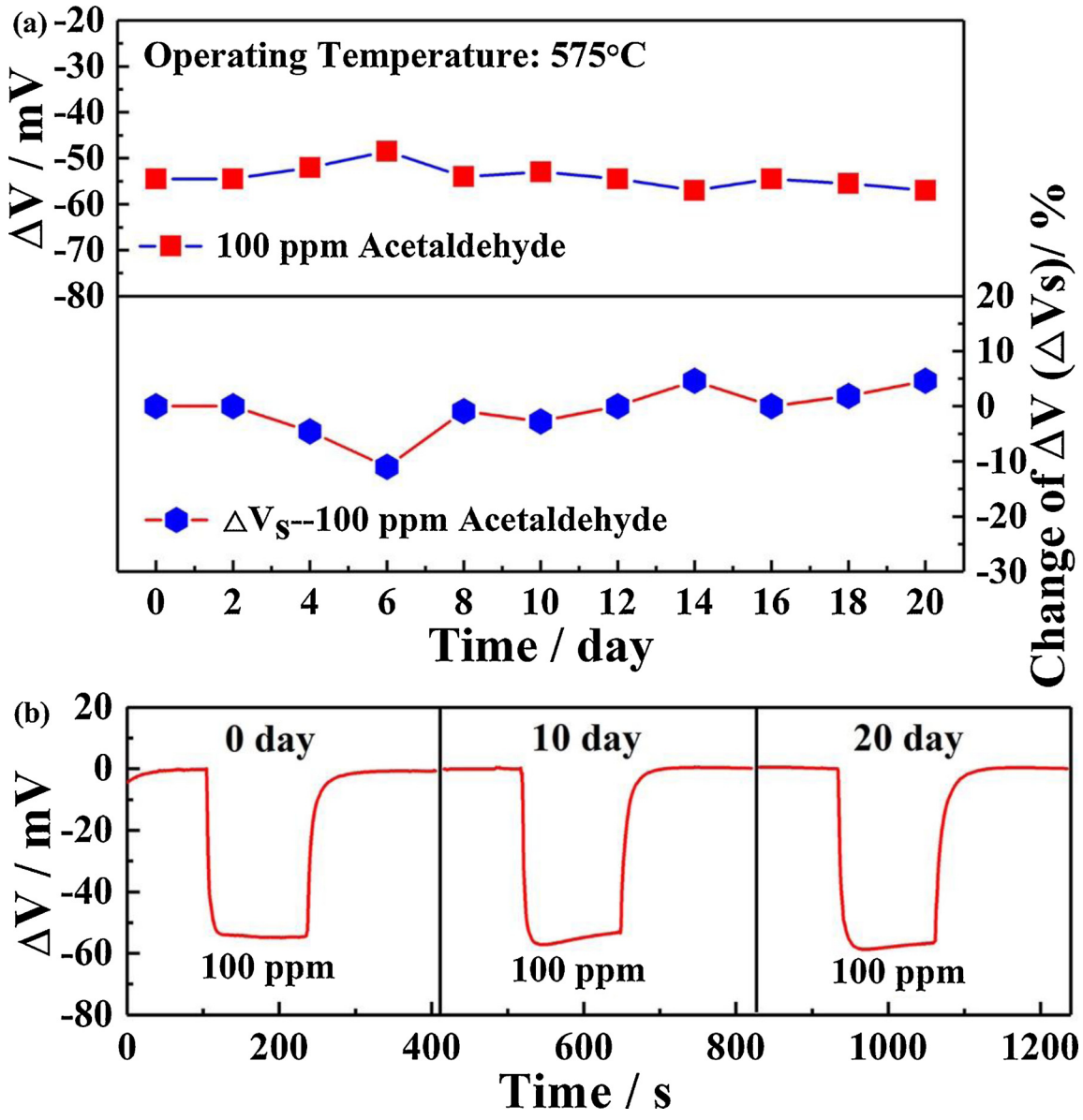

Fig. 9. (a), (b) Long-term stability of the sensor operated at 575 °C for 20 days to 100 ppm acetaldehyde.

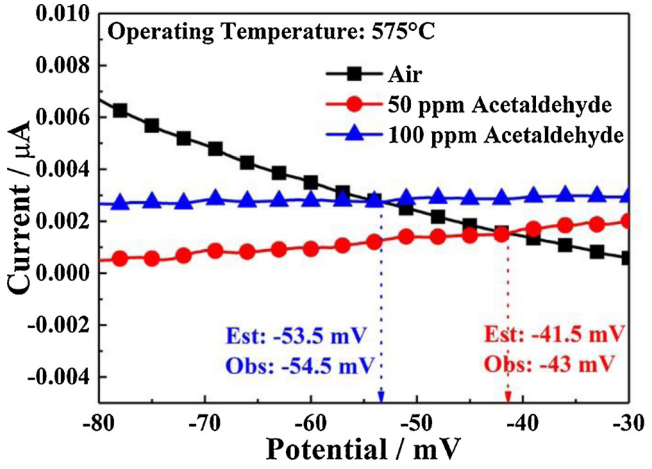

Fig. 10. Polarization curves in air, 50 and 100 ppm acetaldehyde for the sensor using $NiTiO_3$-SE calcined at 1000 °C at 575 °C.

Investigation. **Li Jiang:** Formal analysis, Writing - review & editing. **Lianjing Zhao:** Methodology, Writing - review & editing. **Fangmeng Liu:** Conceptualization, Formal analysis, Methodology, Funding acquisition, Supervision. **Rui You:** Methodology, Writing - review & editing. **Siyuan Lv:** Methodology, Writing - review & editing. **Junming He:** Methodology, Writing - review & editing. **Zijie Yang:** Methodology, Writing - review & editing. **Ao Liu:** Methodology, Writing - review & editing. **Chenguang Wang:** Methodology, Writing - review & editing. **Xu Yan:** Methodology, Writing - review & editing. **Peng Sun:** Methodology, Writing - review & editing. **Geyu Lu:** Conceptualization, Formal analysis, Methodology, Funding acquisition, Supervision, Writing - review & editing.

Declaration of Competing Interest

The authors declare that they have no known competing financial interests or personal relationships that could have appeared to influence the work reported in this paper.

Acknowledgements

This work is supported by the National Natural Science Foundation of China (Nos. 61831011, 61803171, 61520106003, 61722305 and 61833006), Program for Chang Jiang Scholars and Innovative Research Team in University (No. IRT-17R47), National Key Research and Development Program of China (Nos. 2016YFC0207300 and 2016YFC0201002), Application and Basic Research of Jilin Province (20130102010 JC), Young Elite Scientists Sponsorship Program by CAST (2018QN RC001), Program for JLU Science and Technology Innovative Research Team (JLUSTIRT 2017TD-07), China Postdoctoral Science Foundation Funded Project (No. 2018M630322, 2019T120239), Jilin Provincial Science and Technology Development Program (20190103155JH), Jilin Provincial Education Department Science and Technology Project (JJKH20190114KJ), Fundamental Research Funds for the Central Universities.

Appendix A. Supplementary data

Supplementary material related to this article can be found, in the online version, at doi:https://doi.org/10.1016/j.snb.2020.128329.

References

[1] A. Giberti, M.C. Carotta, B. Fabbri, S. Gherardi, V. Guidi, C. Malagu, High-sensitivity detection of acetaldehyde, Sens. Actuators B Chem. 174 (2012) 402–405.
[2] S. Kumar, M. Nayek, A. Kumar, A. Tandon, P. Mondal, P. Vijay, U.D. Bhangale, D. Tyagi, Aldehyde, ketone and methane emissions from motor vehicle exhaust: a critical review, Am. Chem. Sci. J. 1 (2011) 1–27.
[3] A.A. Mohamed, A.T. Mubarak, Z.M.H. Marestani, K.F. Fawy, Highly sensitive and selective catalytic determination of formaldehyde and acetaldehyde, Talanta 74 (2008) 578–585.
[4] J. Jun, Y. Park, C. Lee, Characteristics of a metal-loaded SnO_2/WO_3 thick film gas sensor for detecting acetaldehyde gas, Bull. Korean Chem. Soc. 32 (2011) 1865–1872.
[5] R.D. Williams, H.L. Mason, R.M. Wilder, B.F. Smith, Induced thiamine (Vitamin B1) deficiency and the thiamine requirement of man further observations, Arch. Intern. Med. 69 (1942) 721–738.
[6] D. Klensporf, H.H. Jeleń, Analysis of volatile aldehydes in oat flakes by SPME-GC/MS, Pol. J. Food Nutr. Sci. 14 (2005) 389–395.
[7] X. Guan, E. Rubin, H. Anni, An optimized method for the measurement of acetaldehyde by high-performance liquid chromatography, Alcohol Clin. Exp. Res. 36 (2012) 389–405.
[8] A. Hodgson, P. Jacquinot, L.R. Jordan, P.C. Hauser, Amperometric gas sensors of high sensitivity, Electroanal 11 (1999) 782–787.
[9] K. Hirayama, Y. Sakai, K. Kameoka, K. Nodac, R. Naganawa, Preparation of a sensor device with specific recognition sites for acetaldehyde by molecular imprinting technique, Sens. Actuators B Chem. 86 (2002) 20–25.
[10] P. Rai, Y.T. Yu, Citrate-assisted hydrothermal synthesis of single crystalline ZnO nanoparticles for gas sensor application, Sens. Actuat. B Chem. 173 (2012) 58–65.
[11] Y. Chu, Q. Zhang, Y. Li, Z. Xu, W. Long, A cataluminescence sensor for propionaldehyde based on the use of nanosized zirconium dioxide, Microchim. Acta 181 (2014) 1125–1132.
[12] S.A. Feyzabad, A.A. Khodadadi, M.V. Naseh, Y. Mortazavi, Highly sensitive and selective sensors to volatile organic compounds using MWCNTs/SnO_2, Sens. Actuators B Chem. 166-167 (2012) 150–155.
[13] N. Miura, S. Zhuiykov, T. Ono, M. Hasei, N. Yamazoe, Mixed potential type sensor using stabilized zirconia and $ZnFe_2O_4$ sensing electrode for NO_x detection at high temperature, Sens. Actuators B Chem. 83 (2002) 222–229.
[14] Q. Diao, C. Yin, Y. Liu, J. Li, X. Gong, X. Liang, S. Yang, H. Chen, G. Lu, Mixed-potential-type NO_2 sensor using stabilized zirconia and Cr_2O_3-WO_3 nanocomposites, Sens. Actuators B Chem. 180 (2013) 90–95.
[15] H. Giang, H. Duy, P. Ngan, G. Thai, D. Thu, N. Toan, High sensitivity and selectivity of mixed potential sensor based on Pt/YSZ/$SmFeO_3$ to NO_2 gas, Sens. Actuators B Chem. 183 (2013) 550–555.
[16] P. Elumalai, V. Plashnitsa, Y. Fujio, N. Miura, Stabilized zirconia-based sensor attached with NiO/Au sensing electrode aiming for highly selective detection of ammonia in automobile exhausts, Electrochem. Solid-State Lett. 11 (2008) J79–J81.
[17] F. Liu, R. Sun, Y. Guan, X. Cheng, H. Zhang, Y. Guan, X. Liang, P. Sun, G. Lu, Mixed-potential type NH_3 sensor based on stabilized zirconia and $Ni_3V_2O_8$ sensing electrode, Sens. Actuators B Chem. 210 (2015) 795–802.
[18] I. Lee, B. Jung, J. Park, C. Lee, J. Hwang, C. Park, Mixed potential NH_3 sensor with $LaCoO_3$ reference electrode, Sens. Actuators B Chem. 176 (2013) 966–970.
[19] Y. Guan, C. Yin, X. Cheng, X. Liang, Q. Diao, H. Zhang, G. Lu, Sub-ppm H_2S sensor based on YSZ and hollow balls $NiMn_2O_4$ sensing electrode, Sens. Actuators B Chem. 193 (2014) 501–508.
[20] Y. Fujio, V. Plashnitsa, M. Breedon, N. Miura, Construction of sensitive and selective zirconia-based CO sensors using $ZnCr_2O_4$-based sensing electrodes, Langmuir 28 (2012) 1638–1645.
[21] N. Miura, T. Raisen, G. Lu, N. Yamazoe, Highly selective CO sensor using stabilized zirconia and a couple of oxide electrodes, Sens. Actuators B Chem. 47 (1998) 84–91.
[22] T. Sato, V. Planshnitsa, M. Utiyama, N. Miura, Potentiometric YSZ-based sensor using NiO sensing electrode aiming at detection of volatile organic compounds (VOCs) in air environment, Electrochem. commun. 12 (2010) 524–526.
[23] Y. Suetsugu, T. Sato, M. Breedon, N. Minura, C_3H_6 sensing characteristics of rod-type yttria-stabilized zirconia-based sensor for ppb level environmental monitoring applications, Electrochim. Acta 73 (2012) 118–122.
[24] Y. Fujio, V. Plashnitsa, P. Elumalai, N. Miura, Stabilization of sensing performance for mixed-potential-type zirconia-based hydrocarbon sensor, Talanta 85 (2011) 575–581.
[25] F. Liu, Y. Guan, R. Sun, X. Liang, P. Sun, F. Liu, G. Lu, Mixed potential type acetone sensor using stabilized zirconia and $M_3V_2O_8$ (M: Zn Co and Ni) sensing electrode, Sens. Actuators B Chem. 221 (2015) 673–680.
[26] H. Han, T. Kim, S. Kim, S. Oh, C. Park, Fast initializing solid state electrochemical carbon dioxide sensor fabricated by a tape casting technique using yttria stabilized zirconia and sodium beta alumina heterojunction, Sens. Actuators B Chem. 248 (2017) 856–861.
[27] T. Ueda, H. Abe, K. Kamada, S. Bishop, H. Tuller, T. Hyodo, Y. Shimizu, Enhanced sensing response of solid-electrolyte gas sensors to toluene: role of composite Au/metal oxide sensing electrode, Sens. Actuators B Chem. 252 (2017) 268–276.
[28] T.-W. Kim, J.-W. Kim, S.-M. Lee, C.-O. Park, Humidity effects on the initial stabilization behavior of a solid electrochemical CO_2 sensor, Sens. Actuators B Chem. 295 (2019) 65–69.
[29] H. Fan, Y. Zeng, H. Yang, X. Zheng, L. Liu, T. Zhang, Preparation and gas sensitive properties of ZnO-CuO nanocomposites, Acta Phys. Chem. Sin. 24 (2008) 1292–1296.
[30] K.P. Lopes, L.S. Cavalcante, A.Z. Simões, J.A. Varela, E. Longo, E.R. Leite, $NiTiO_3$ powders obtained by polymeric precursor method: synthesis and characterization, J. Alloys. Compd. 468 (2009) 327–332.
[31] T. Zima, A. Smirnov, Synthesis and characterization of one-dimensional Co-doped titanate nanostructures prepared in the presence of chitosan, Mater. Res. Bull. 62 (2015) 106–113.
[32] R. Tursun, J. Tan, Q. Yu, Y. Su, L. Xiao, Effect of annealing temperature on the structural and solar heat shielding performance of $NiTiO_3$ nanopowder, Sol. Energy 159 (2018) 697–703.
[33] A. Sambandam, L.-V. Teresa, J.W. Jerry, Sonochemical synthesis of mesoporous $NiTiO_3$ Ilmenite nanorods for the catalytic degradation of tergitol in water, Ind. Eng. Chem. Res. 54 (2015) 2983–2990.
[34] G. Yang, W. Chang, W. Yan, Fabrication and characterization of $NiTiO_3$ nanofibers by sol-gel assisted electrospinning, J. Solgel Sci. Technol. 69 (2014) 473–479.
[35] F. Liu, X. Yang, B. Wang, Y. Guan, X. Liang, P. Sun, G. Lu, High performance mixed potential type acetone sensor based on stabilized zirconia and $NiNb_2O_6$ sensing electrode, Sens. Actuators B Chem. 229 (2016) 200–208.
[36] N. Miura, M. Nakatou, S. Zhuiykov, Impedance-based total-NO_x sensor using stabilized zirconia and $ZnCr_2O_4$ sensing electrode operating at high temperature, Electrochem. Commun. 4 (2002) 284–287.
[37] M. Stranzenbach, E. Gramckow, B. Saruhan, Planar, impedance-metric NO_x- sensor with spinel-type SE for high temperature applications, Sens. Actuators B Chem. 127 (2007) 224–230.
[38] H. Jin, Y. Huang, J. Jian, Sensing mechanism of the zirconia-based highly selective NO sensor by using a plate-like Cr_2O_3 sensing electrode, Sens. Actuators B Chem. 219 (2015) 112–118.
[39] N. Miura, M. Nakatou, S. Zhuiykov, Impedancemetric gas sensor based on zirconia solid electrolyte and oxide sensing electrode for detecting total NO_x at high temperature, Sens. Actuators B Chem. 93 (2003) 221–228.
[40] L. Wu, J. Xia, W. Shi, D. Jiang, Q. Li, NO_2-sensing properties of $La_{0.65}Sr_{0.35}MnO_3$ synthesized by self-propagating combustion, Ionics 22 (2016) 927–934.
[41] M. Kasalizadeh, A.A. Khodadadi, Y. Mortazavia, Coupled metal oxide-doped Pt/SnO_2 semiconductor and yittria-stabilized zirconia electrochemical sensors for detection of VOCs, J. Electrochem. Soc. 160 (2013) B218–B224.
[42] G. Lu, N. Miura, N. Yamazoe, High-temperature hydrogen sensor based on stabilized zirconia and a metal oxide electrode, Sens. Actuators B Chem. 35-36 (1996) 130–135.
[43] N. Miura, J. Wang, M. Nakatou, P. Elumalai, M. Hasei, NO_X sensing characteristics of mixed-potential-type zirconia sensor using NiO sensing electrode at high temperature, Electrochem. Solid-State Lett. 8 (2005) H9–H11.
[44] N. Miura, G. Lu, N. Yamazoe, Progress in mixed-potential type devices based on solid electrolyte for sensing redox gases, Solid State Ion. 136-137 (2000) 533–542.
[45] N. Miura, T. Sato, S. Anggraini, H. Ikeda, S. Zhuiykov, A review of mixed-potential type zirconia-based gas sensors, Ionics 20 (2014) 901–925.

Jing Wang received her B.S. degree in applied chemistry in 2009 and the M.S. degree in polymer chemistry and physics in 2012 from Northeast Forestry University in China. She is now a Ph.D. student at College of Electronic Science and Engineering, Jilin University, China. Her current research is solid electrolyte gas sensor.

Li Jiang received the B.Eng. degree in department of electronic science and technology in 2019. He is currently studying for his M.E. Sci. degree in College of Electronic Science and Engineering, Jilin University, China.

Lianjing Zhao received her M.S. degree in 2013 from Jilin University, China. She is currently studying for her Ph.D. degree in College of Electronic Science and Engineering,

Jilin University. Her research interests mainly focus on the development of the functional nanomaterials and their applications in chem/biosensor.

Fangmeng Liu received his PhD degree in 2017 from College of Electronic Science and Engineering, Jilin University, China. Now he is an associate Professor of Jilin University, China. His current research interests include the application of functional materials and development of solid state electrochemical gas sensor and flexible device.

Rui You received his B.S. degree from Department of Opto-Electronic Engineering in 2013, Changchun University of Science and Technology, Changchun, China. He is now a Ph.D. student at the Department of Precision Instrument at Tsinghua University, Beijing, China. Currently his research interests mainly include gas sensor and application of MEMS process.

Siyuan Lv entered Jilin University in 2016. Now she is studying for her B.Eng. degree in department of electronic science and technology.

Junming He received the B.Eng. degree in department of electronic science and technology in 2017. She is currently studying for her M.E. Sci. degree in College of Electronic Science and Engineering, Jilin University, China.

Zijie Yang received the B.S. degree in department of electronic science and technology in 2017. He is currently studying for his M.E. Sci. degree in College of Electronic Science and Engineering, Jilin University, China.

Ao Liu received the B.S. degree in department of electronic science and technology in 2018. He is currently studying for his M.E. Sci. degree in College of Electronic Science and Engineering, Jilin University, China.

Chenguang Wang received his PhD degree from the College of Chemistry, Jilin University in 2013. He then joined the Institute of Transformative Bio-Molecules, Nagoya University as a postdoctoral fellow. In 2019, he joined the College of Electronic Science and Engineering, Jilin University as a professor. His research interests focus on the design and synthesis of organic fluorescent molecules and their applications in fluorescence bio-imaging.

Xu Yan received his M.S. degree in 2013 from Nanjing Agricultural University. He joined the group of Prof. Xingguang Su at Jilin University and received his Ph.D. degree in June 2017. Since then, he did postdoctoral work with Prof. Geyu Lu. Currently, his research interests mainly focus on the development of the functional nanomaterials for chem/bio sensors.

Peng Sun received his PhD degree from the Electronics Science and Engineering department, Jilin University, China in 2014. Now, he is engaged in the synthesis and characterization of the semiconducting functional materials and gas sensors.

Geyu Lu received the B.Sci. degree in electronic sciences in 1985 and the M.S. degree in 1988 from Jilin University in China and the Dr. Eng. degree in 1998 from Kyushu University in Japan. Now he is a professor of Jilin University, China. His current research interests include the development of chemical sensors and the application of the function materials.